3P-21

Proceedings of Symposium on Ultrasonic Electronics, Vol. 31 (2010) pp. 497-498
6-8 December, 2010

Measurement Point Reduction for Acoustic Imaging in Square Billet

超音波による角鋼片断層映像における計測点数の少数化

Hideto Mitsui‡, Koichi Mizutani, Naoto Wakatsuki, and Yoko Norose (Univ. Tsukuba)
三井 秀人‡, 水谷 孝一, 若槻 尚斗, 野呂瀬 葉子（筑波大院・シス情工）

1. Introduction

Square billets are manufactured by continuous casting and processed into many metal products such as plate and pipe. In casting process, defects are caused by remaining inclusions and stress during cooling and extrusion in the billets.[1] We treat holes down to 2 mm in diameter as the defects. Defect detection is important for quality improvement of the billets and metal products. Nondestructive testing with ultrasound is efficient for the detection.

We have proposed a method to detect the defects using time-of-flight (TOF) of longitudinal waves[2,3] instead of pulse echo method. The TOF is measured by the transmission method. Apparent sound velocity distribution, which is different from actual sound velocity of the billet, is reconstructed using ultrasonic computerized tomography (CT). The defects are visualized as a decrease in apparent sound velocity because the TOF increases owing to diffraction of ultrasonic waves at the defects.

In these papers, the measurement points on one side were fixed to 50, which were so large that measurement time took long time. If the measurement points are reduced while the visualization ability of defects is maintained, the measurement time becomes short. In this paper, a relationship between the number of measurement points and visualization ability of defects is evaluated by calculation, which is validated based on ray theory.[4]

2. Principles of Defect Visualization

Transmitter and receiver are set on the billet surface and the longitudinal waves are measured using the transmission method. The TOF of the diffracted wave at the defect is larger than that of the direct wave. We detect the defect to utilize the TOF difference, which means increase in TOF, because it contains information relating to defect existence.

The apparent sound velocity is reconstructed from the TOF difference. The apparent sound velocities at the defects areas are lower than those of defect-free areas because the TOF increases owing to the diffraction at the defects. Therefore, a decrease in the apparent sound velocity indicates the existence and location of defects. **Figure 1** shows a schematic view of billet, transducer, and projection used in CT. The projection, $p(X,\theta)$, which is defined as the TOF difference, is given by

$$p(X,\theta) = T(X,\theta) - \frac{L(X,\theta)}{c}, \qquad (1)$$

where $T(X,\theta)$ and $L(X,\theta)$ denote the TOF and length of the propagation path in the Y-direction passing through point (X,θ), respectively. In addition, c denotes the sound velocity in the billet. The apparent sound velocity distribution is reconstructed from the projection using filtered back-projection. To use this method, the projection at equal intervals is required. However, the intervals of obtained projection are unequal. Therefore, the projection at equal intervals is calculated from the obtained projection using cubic spline interpolation.[5] A range between the projection after interpolation and obtained projection is increased as the measurement points are decreased. Otherwise, the visualization ability of defects is reduced as the range is increased.

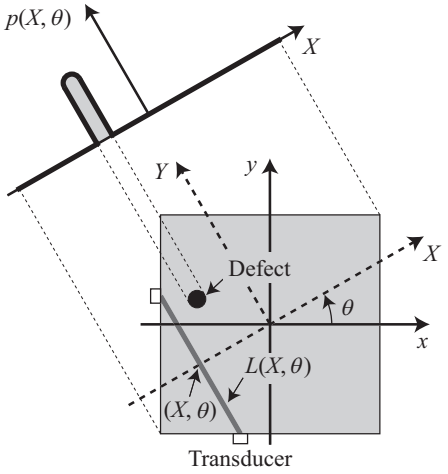

Fig. 1 Schematic view of billet, transducer, and projection used in CT.

3. Simulation Results

Figure 2 shows a simulation setup. The square billet is assumed to duralumin and its size, $(2l)^2$, is 100 × 100 (mm^2). The sound velocity of the billet, c, is about 6320 m/s. The origin is taken at the center of the billet. The transducers are set on

{mizutani, wakatuki}@iit.tsukuba.ac.jp

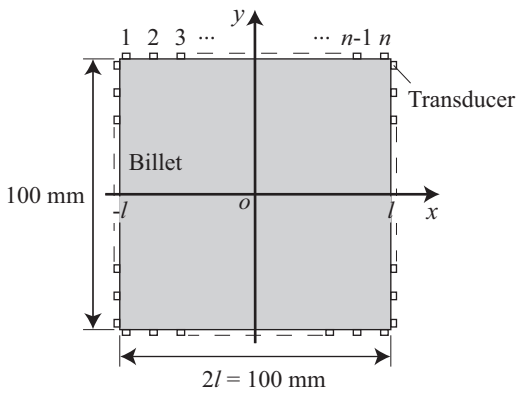

Fig. 2 Simulation setup.

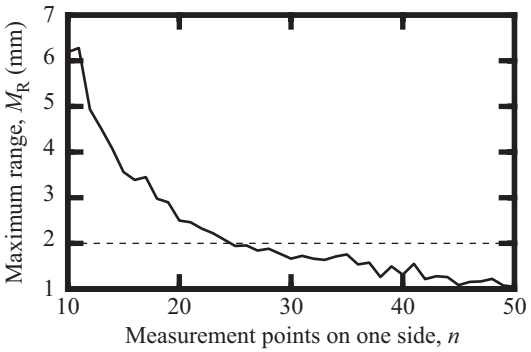

Fig. 3 Maximum range, M_R, in measurement points on one side, n, obtained by ray theory.

the billet surface at equal intervals. The number of measurement points on one side is defined as n. The number of TOF data is equal to the number of combinations of the transmitter and receiver on arbitrary sides subtracted by the number of combinations of those which share a side. Therefore, the number of TOF data, η, is given by

$$\eta = {}_{4n}\mathrm{C}_2 - 4\,{}_n\mathrm{C}_2 . \quad (2)$$

The TOF of each path is obtained by the ray theory.

The projection of TOF data obtained from j-th ($0 \le j \le \eta$) transducer combination is defined as $p(X_j, \theta_j)$. In addition, the projection after interpolation is defined as $p(a\Delta X, b\Delta\theta)$. Here, ΔX and $\Delta\theta$ denote the lengths of mesh grid in X and θ coordinates, respectively, and their values are 2 mm and $\pi/90$ (rad). The range between $(a\Delta X, b\Delta\theta)$ and (X_j, θ_j), $R_{a,b}$, is given by

$$R_{a,b} = \min\sqrt{\left(a\Delta X - X_j\right)^2 + \left(b\Delta\theta - \theta_j\right)^2}\ ,$$
$$\left(-\sqrt{2}l \le a\Delta X \le \sqrt{2}l,\quad 0 \le b\Delta\theta < \pi\right). \quad (3)$$

The maximum range of $R_{a,b}$ is defined as M_R.

$$M_R = \max\left(R_{a,b}\right) . \quad (4)$$

Figure 3 shows the maximum range, M_R, in measurement points on one side, n. The maximum range is decreased as the measurement points one side is increased. It is expected that the defect down to 2 mm in diameter may be visualized if the maximum range is less than 2 mm, which meets the sufficient condition for the interpolation. The maximum range at n = 25 is 1.94 mm. **Figure 4** shows setup and visualized images of defect. Figure 4(a) shows the setup of billet and defect. The defect is located at (x, y) = (32, 42) (mm), which is the same as the location of maximum range in n = 25. In this location, it is the most difficult to visualize the defect. The diameter of defect is 2.0 mm. Figures 4(b)–4(d) show the visualized images of defect at n = 50, 25, and 15, respectively. The gray scale indicates the apparent sound velocity. In Fig 4(d), the defect cannot be visualized because the response of defect in image is less than that of artifacts. In Figs. 4(b) and 4(c), the defect was visualized and its location approximately agrees with the actual location.

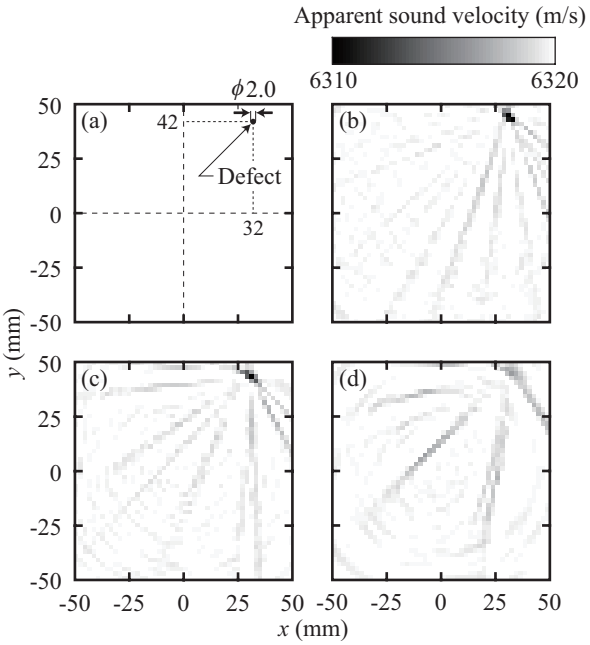

Fig. 4 Setup and visualized images of defects by ray theory. (a): Setup. (b): n = 50. (c): n = 25. (d): n = 15.

4. Conclusions

The relationship between the number of measurement points and visualization ability of defects was evaluated by calculation. As a result, the defect was visualized although the measurement points on one side were reduced by 25 while the visualization result of defects was maintained.

References

1. H. Yamaguchi, N. Matsubara, K. Fujisawa, and S. Matsumoto: Tetsu to Hagane **70** (1984) 1210.
2. H. Mitsui, K. Mizutani, and N. Wakatsuki: Jpn. J. Appl. Phys. **48** (2009) 07GD05.
3. H. Mitsui, K. Mizutani, and N. Wakatsuki: Jpn. J. Appl. Phys. **49** (2009) 07HC13.
4. Y. Sato, K. Mizutani, N. Wakatsuki, and T. Nakamura: Jpn. J. Appl. Phys. **47** (2008) 4354.
5. A. Minamide, K. Mizutani, and N. Wakatsuki: Jpn. J. Appl. Phys. **48** (2009) 07GC02.